Fracture Mechanics of Concrete Structures, de Borst et al (eds) © 2001 Swets & Zeitlinger, Lisse, ISBN 90 2651 825 0

Length Scales of Fiber Reinforced Cementitious Composites – a Review

E.Chuang, M.Overland, & F.-J.UIm
Massachusetts Institute of Technology, Cambridge, Massachusetts, USA

Various models have been used by researchers to describe the tensile behavior of fiber reinforced cementitious composites, particularly the fiber-matrix interaction during loading. This paper examines some models using assorted mathematical methods including dimensional analysis and variational methods. The examination yields greater insight into the behavior of these materials, especially at the point of failure. Furthermore, length scales related to these materials are discussed, which show that high performance cementitious composites (HP2C) are, from a mechanical point of view, a well designed match of two materials and their interactions.

1 INTRODUCTION

It has long been recognized that the reinforcement of cementitious materials with fibers, whether steel, glass, or plastic, is an effective method for improving the intrinsic ductility of the matrix. Fibers improve ductility by dissipative mechanisms in the vicinity of the crack tip, which stabilizes crack activating growth (Rossi et al. 1986). Once the brittle matrix has cracked, the overall composite behavior is governed by debonding and frictional mechanisms that develop along the fiber-matrix interface (see Figure 1). Along with these interface mechanisms, fibers are pulled out of the matrix and/or yield (see, for instance, Gopalaratnam & Shah 1987). The energy that is dissipated by these plastic, fracture, and frictional mechanisms increases the overall ductility of the composite material. The critical nature of this micro-mechanical behavior on failure mode of fiber reinforced cementitious composites (FRCC) prompted intensive research activities aimed at optimizing the composite material behavior through mechanistic models of the fiber pullout behavior. A lot has been learned ever since Kelly identified a critical fiber length for an optimized matrix-fiber composite behavior (Kelly 1964).

At present, a new generation of high performance cementitious composites (HP2C) is emerging on the market with chemically and mechanically fine tuned strength, ductility, and durability properties. At this stage, it is useful to review the different length scales which determine the mechanical performance of FRCC and HP2C. This is the main focus of this paper.

2 GOVERNING EQUATIONS

The loading and pullout behavior of a single fiber is usually modeled from known parameters, including the material behavior of the fiber, the matrix, and the matrix-fiber interface. These models often assume that through the elastic loading phase, the fiber and matrix are bonded by the interface, which transfers stresses from the fiber to the matrix. Assuming the fiber and matrix have not failed, an interfacial crack forms and propagates creating a debonding zone as the load increases. Shear stresses can also be transferred through the debonding zone through frictional stresses. When the fiber becomes fully debonded, the fiber begins to slip as the imposed deflection increases. As slip increases, the fiber-matrix contact zone decreases. This causes the load transfer capability to decrease.

There are three distinct phases in the loading and pullout of the fiber: the elastic stage, the onset of failure and/or yielding, and the fiber slip stage (if any). The first two phases will be considered using dimensional analyses of various FRCC models. Two

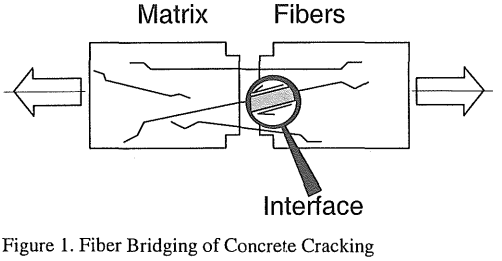

Figure 1. Fiber Bridging of Concrete Cracking

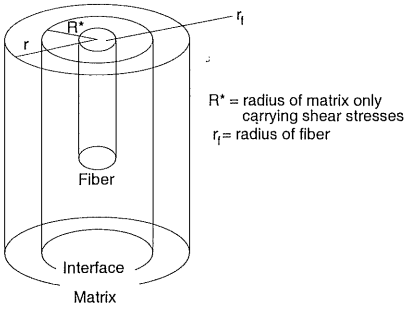

Figure 2. The Three-Body Matrix-Interface-Fiber System (Budiansky et al. 1985).

aspects in particular will be examined: transfer of elastic stresses along the fiber-matrix interface, and onset of FRCC yielding or failure. One of the simplest micro-mechanical systems for fiber pullout studies is the three-body model introduced by Budiansky et al. (1985) shown in Figure 2. This fiber loading model assumes that the fibers are aligned and regularly distributed in the matrix. The free body is composed of a fiber (fiber radius r_f), and a matrix layer, separated by an interface layer of finite thickness $e = R^* - r_f$. Let $P = \sigma_f A_f$ be the normal stress resultant at the free end of the fiber (or fiber force) over the fiber section $A_f = \pi r_f^2$, σ_f the average longitudinal fiber stress, and τ_0 the shear stress at the fiber perimeter at $r = r_f$. Elementary force equilibrium over a fiber element of length dz gives:

$$\frac{d\sigma_f}{dz} = -\frac{2\tau_0}{r_f} \tag{1}$$

and the momentum balance in the matrix reduces to:

$$r\frac{d\sigma_m}{dz} + \frac{d(r\tau_m)}{dr} = 0 \tag{2}$$

with $\sigma_m = \sigma_{zz}$ the longitudinal stress in the direction of the fiber alignment, and $\tau_m = \sigma_{zr}$ the shear stress. In the interface zone $r \in]r_f, R^*[$, the longitudinal stress is assumed to be zero, which requires that the shear stress decreases with 1/r, i.e. from integration of the last term of Equation (2), $\tau_m(r,z)/\tau_0(z) = r_f/r$.

With Equation (1) and (2) in hand, the various fiber loading models differ only in the constitutive law applied for the three components of the three-body system.

2.1 Elastic Embedment Length

The elastic load transfer from the fiber to the matrix requires a certain embedment length. It is generally assumed that the shear stress at the interface obeys an elastic interface constitutive relation of the form (see Aveston et al. 1971; Leung & Li 1991, among many others):

$$\tau_0(z) = -k[[w]] = -k(w_f(z) - w_m(z)) \tag{3}$$

where $[[w]] = w_f(z) - w_m(z)$ is the displacement between the fiber (subscript f) and the matrix (subscript m). The slip modulus, k (of dimension $[k] = MT^{-2}L^{-2}$), is defined to be the shear stress per unit of displacement between the fiber and matrix. An estimate of this slip behavior has been given by Budiansky et al. (1985), by assuming a continuous elastic behavior of the matrix constituting the interface zone:

$$r\frac{\partial w(r,z)}{\partial r} = 2\varepsilon_{rz} = \frac{\tau_m(r,z)}{\mu_m} = \frac{\tau_0(z)}{\mu_m}\frac{r_f}{r} \tag{4}$$

where $\mu_m = E_m/2(1+\nu_m)$ is the shear modulus of the matrix, E_m the Young's modulus of the matrix, and ν_m the Poisson's ratio of the matrix. Integration over r, with the boundary conditions $w(r = r_f,z) \equiv w_f(z)$ and $w(r = R^*,z) \equiv w_m(z)$ yields the slip modulus:

$$k = \frac{\mu_m}{r_f \ln\left(R^*/r_f\right)} \tag{5}$$

Budiansky et al. (1985) also provide an estimate for the thickness of the interface zone:

$$\ln(R^*/r_f) = -\frac{2\ln V_f + V_m(3 - V_f)}{4V_m^2} \tag{6}$$

where V_f and $V_m = 1 - V_f$ denote respectively the volume fraction of fibers and matrix of the composite. For FRCC and HP2C the maximum fiber volume ratio is often restricted to $V_f = 1 - 5\%$ in order to maintain reasonable workability. Applying this to Equation (6) gives:

$$R^*/r_f \approx 2.5 - 5 \tag{7}$$

This shows that the thickness e of the interface zone in FRCC and HP2C is typically on the order of 2-4 times the fiber radius. Given the small values of fiber radius of $r_f = 0.3 - 0.5$ mm, e is on the order of 1 mm, which justifies a posteriori the lumped interface behavior in form of Equation (3). This reduces the 3-body system to a 2-body system separated by a (fixed) surface of discontinuity, where the displacement is discontinuous, but the shear stress continuous, i.e. $\tau_m(r = r_f) = \tau_0$.

For this two-body elastic system, deriving Equations (1) and (3) yields:

$$\frac{d^2\sigma_f}{dz^2} - \frac{2k}{r_f E_f}\sigma_f = -\frac{2k}{r_f}\varepsilon \tag{8}$$

where we used an elastic fiber behavior, $\sigma_f = P/A_f = E_f \partial w_f / \partial z$, with E_f the elastic modulus of the fiber. $\varepsilon(z) = \frac{\partial w_m}{\partial z}\big|_{r=r_f}$ is the longitudinal strain on the matrix side of the interface, which is zero at the crack face., i.e. $\varepsilon(z=0) = 0$, and increases along z due to

Table 1. Typical Values of Fiber and Concrete Material Parameters (Lim et al 1987, Rossi 1997).

Steel Fiber	
Tensile Strength	500-1200 MPa
Tensile Modulus	200 GPa
Radius	.3-.5 mm
Total Length	30-50 mm
Embed. Length	15-25 mm

Normal Strength Concrete	
Fiber Volume	1-3%
Tensile Strength	2-5 MPa
Shear Strength	2-5 MPa
Bond Strength	2-7 MPa
Tensile Modulus	20-25 GPa
Shear Modulus	10-15 GPa
Slip Modulus	1-3 GPa/m
FRCC Modulus	25-30 MPa
Fracture Energy	5 J/m^2

High Strength Concrete	
Fiber Volume	3-5%
Tensile Strength	8-20 MPa
Shear Strength	8-20 MPa
Tensile Modulus	50-60 GPa
Shear Modulus	20-25 GPa
Fracture Energy	30 J/m^2

the fiber-matrix stress transfer over the common interface, until the strain in both matrix and fiber have the same value. Without solving Equations (8) and (2), by applying appropriate boundary conditions, it appears that the elastic stress transfer into the matrix is governed by a characteristic length:

$$\ell_s = \sqrt{\frac{r_f E_f}{2k}} \propto (E_f/\mu_m)^{1/2} \tag{9}$$

The illustration is straightforward by considering a linear transform of the spatial coordinate $z = \delta \ell_s \bar{z}$, where $\bar{z} \equiv O(1) \leftrightarrow \delta = z/\ell_s$. Using Equation (8) gives:

$$\left(\frac{1}{\delta^2}\right)\frac{\partial^2 \sigma_f}{\partial z^{-2}} = \sigma_f - E_f \varepsilon \tag{10}$$

Inspecting the previous equation for $\delta^2 >> 1$ shows that the fiber strain far from the crack face reaches the same value as the matrix, indicating a perfect elastic slip-less behavior of the composite behavior:

$$\delta^2 >> 1 \leftrightarrow z >> \ell_s: \quad \sigma_f^{\infty} = E_f \varepsilon^{\infty} \leftrightarrow \varepsilon^{\infty} = \frac{\partial w_m}{\partial z} = \frac{\partial w_f}{\partial z} \tag{11}$$

As it is well known from homogenization theories of composite materials, this strain compatibility represents a maximum elastic energy state, as both matrix and fibers deform in the same way, and can be considered, therefore, as an optimized composite behavior.

Conversely, for $\delta^2 << 1$, according to Equation (1) and (10), the embedment length is too small to transfer stresses from the fiber into the matrix. In between these limit cases, the gauge length ℓ_s given by Equation (9) defines a minimum required embedment length for an elastic stress transfer of fiber stresses bridging a crack, requiring a minimum fiber length L_f, typically

$$L_f/2 > 4 - 5 \times \ell_s \leftrightarrow \delta^2 = 16 - 25 >> 1 \tag{12}$$

For FRCC and HP2C, typical values of fiber and concrete material parameters, summarized in Table 1, are V_f = 1-5%, $r_f = 0.3 - 0.5$ mm, $E_f = 200$ GPa, $\mu_m = 10 - 15$ GPa for FRCC and $\mu_m = 20 - 25$ GPa for HP2C; thus

$$\frac{\ell_s}{r_f} = \sqrt{\frac{E_f \ln(R^*/r_f)}{2\mu_m}} = 2 - 4 \tag{13}$$

Hence, a fiber length to fiber radius ratio on the order of $L_f/r_f > 16$ - 40 is required to ensure an optimized elastic stress transfer in cementitious composites. This is generally the case, given typical fiber lengths employed for FRCC and HP2C, for which $L_f/r_f \sim 30 - 150$.

2.2 *Anchorage Strength Length*

The elastic stress transfer from the fiber to the matrix is restricted by the strengths of the composite components, fiber, matrix and interface. As a first approach, we will focus only on the strength of fiber and interface, by introducing in addition to the equilibrium condition (1) the following strength criteria:

$$\sigma_f - \sigma_{fu} \le 0; \quad \tau - \tau_u \le 0 \tag{14}$$

This is roughly along the lines of assumptions that led Kelly in 1964 to the derivation of a critical embedment length:

$$\ell_a = \frac{\sigma_{fu} r_f}{\tau_u} \tag{15}$$

To reveal its physical significance, it is useful to re-derive Kelly's length scale from first principles of dimensional analysis (Barenblatt 1996), by introducing the following linear transformations of all parameters and functions involved in Equations (1) and (14):

$$z = Zz'; \quad r_f = R_f r_f'; \quad \sigma_f = \Sigma_f \sigma_f'; \quad \tau_0 = T_0 \tau_0'; \quad \sigma_{fu} = \Sigma_{fu} \sigma_f'; \quad \tau_u = T_u \tau_u' \tag{16}$$

where $z', r_f', \sigma_f', \tau_0', \sigma_{fu}'$ and τ_u' are the dimensionless

counterparts of parameters z, r_f, σ_f, τ_0, σ_{fu} and τ_u of dimension $Z, R_f, \Sigma_f, T_0, \Sigma_{fu}$ and T_u. Use of (16) in (1) and (14) yields:

$$\left(\frac{R_f \Sigma_f}{Z T_0}\right)\frac{\partial \sigma_f'}{\partial z'} = -\frac{2\tau_0'}{r_f'} \tag{17}$$

$$\left(\frac{\Sigma_f}{\Sigma_{fu}}\right)\sigma_f' - \sigma_{fu}' \le 0; \quad \left(\frac{T_0}{T_u}\right)\tau' - \tau_u' \le 0 \tag{18}$$

Dimensional homogeneity of these two equations requires:

$$\frac{\Sigma_f}{\Sigma_{fu}} = \frac{T_0}{T_u} = \frac{R_f \Sigma_f}{Z T_0} = 1 \tag{19}$$

and leads to the identification of the following dimensionless parameters:

$$\pi_1 = \frac{\sigma_f}{\sigma_{fu}} = \frac{\sigma_f'}{\sigma_{fu}'}; \quad \pi_2 = \frac{\tau_0}{\tau_u} = \frac{\tau_0'}{\tau_u'}; \quad \pi_3 = \frac{z}{r_f \sigma_f / \tau_0} \tag{20}$$

Since one can always redefine invariants as product and power functions of the previously identified invariants π_1, π_2 and π_3, we can choose the following:

$$\bar{\sigma}_f = \pi_1 = \frac{\sigma_f}{\sigma_{fu}}; \quad \bar{\tau} = \pi_2 = \frac{\tau_0}{\tau_u};$$
$$\bar{z} = \pi_1 \pi_2^{-1} \pi_3 = \frac{z}{\ell_a} \tag{21}$$

where the gauge length ℓ_a normalizing the z-coordinate is Kelly's critical length scale given by (15). Proceeding as in the previous section, we let $2z = \delta \ell_a \bar{z}$ with $\bar{z} \equiv O(1) \leftrightarrow \delta = z/\ell_s$ in Equations (1) and (14):

$$\frac{\partial \bar{\sigma}_f}{\partial \bar{z}} = -\delta \bar{\tau}; \quad \bar{\sigma}_f - 1 \le 0; \quad \bar{\tau} - 1 \le 0 \tag{22}$$

The dimensionless forms in Equation (22) indicate that the maximum stress transfer occurs for $\delta = 1$, for which the strength capacity of both fiber and interface can be activated. In turn, for $\delta >> 1$, $\bar{\tau} = 0$;

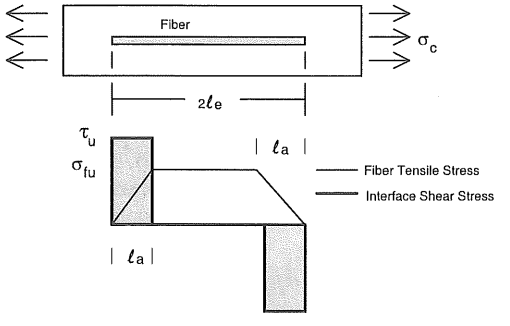

Figure 3. Stresses in the Fiber and the Interface at the Point of Composite Yielding (Kelly 1964)

this implies for long fibers $L_f/2 >> \ell_a$, that the composite behavior is dominated by fiber yielding, confining anchorage effects into small zones at the end of the fiber over a length ℓ_a. This is shown in Figure 3, and is similar to steel bar reinforcement of reinforced concrete structures, in which the anchorage length of the bar is short in comparison to the entire bar. Conversely, for $\delta << 1$, associated with short fiber lengths $L_f/2 << \ell_a$, the composite behavior is dominated by interface strength restrictions, with a negligible stress gradient $\partial \sigma_f / \partial z \to 0$. Therefore, for short fibers, fiber pullout is expected to occur before significant axial stress develops in the fiber.

For normal strength fiber reinforced cementitious composites (FRCC) Kelly's critical length is on the order of:

$$\text{FRCC}: \ell_a = 50 - 150\text{mm} \tag{23}$$

This indicates that the most common failure mode of FRCC with typical fiber lengths $L_f < 50$ mm $<< 2\ell_a$, will be fiber slippage and pullout, not fiber rupture, as the critical anchorage lengths are rarely achieved. Therefore, the strength of the fibers is underutilized, and fiber slippage occurs before a significant fraction of the fiber strength is activated. One way to address this problem is to use hooked fibers. Alternatively, one could employ lower strength fibers with strengths σ_{fu} ~ 100 MPa to better suit the low bond strength of normal strength concretes.

However, for high strength cementitious composites,

$$\text{HP2C}: \ell_a = 10 - 40\text{mm} \tag{24}$$

This is a better material match for typical fibers lengths employed in HP2C, as $L_f/2\ell_a$ approaches unity. Therefore, the amount of energy in HP2C, which is dissipated by both fiber slippage and fiber yielding, is larger than in FRCC, and contributes to the enhanced ductility property of HP2C. In the case of HP2C, hooked end fibers would not be necessary.

2.3 Radial Influence Zone

To this point the restricted matrix strength domain has been disregarded. Supporting this assumption is the fact that the shear is maximum at the interface, and restricted through introduction of strength criterion (14b). However, one may argue that the stress in the matrix is not a pure shear stress state, but involves, at least, a longitudinal stress $\sigma_m = \sigma_{zz}$ and a shear component $\tau_m = \sigma_{zr}$. When these stresses reach the strength of the matrix, failure may not necessarily be initiated at the interface, but at a certain distance from the fiber in the matrix. To evaluate this effect, we consider as governing equations, the equilibrium relations (1) and (2), together with the condition of stress continuity at the steel-matrix interface:

$$r = r_f : \tau_m(r_f) = \tau_0 \tag{25}$$

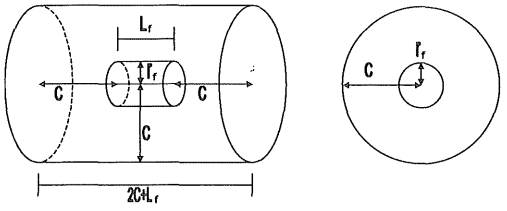

Figure 4. Fiber Spacing in a Representative Cylinder

and, in addition to strength criteria (14), a tension cut-off criterion for the matrix, reading:

$$\frac{\sigma_m}{2}+\sqrt{\left(\frac{\sigma_m}{2}\right)^2+\tau_m^2}-\sigma_{mu}\le 0 \tag{26}$$

Here, σ_{mu} is the tensile strength of the matrix. In addition to the invariants (20), dimensional homogeneity of the whole set of equations allows us to manipulate the following additional invariants:

$$\pi_4=\frac{\sigma_m r}{\tau_m z};\quad \pi_5=\frac{r}{r_f};\quad \pi_6=\frac{\tau_m}{\tau_0};\quad \pi_7=\frac{\sigma_m}{\sigma_{mu}};\quad \pi_8=\frac{\tau_m}{\sigma_{mu}} \tag{27}$$

With similar dimensional arguments as previously employed, recombining invariants (i.e., $\bar{z}=z/\ell_a=\pi_1\pi_2^{-1}\pi_3/2$, or $\bar{z}=z/\ell_a=\pi_1\pi_3\pi_6\pi_8^{-1}/2$), Kelly's critical length scale for plastic anchorage remains highly relevant, but depends now on the bond-strength-to-tensile-strength ratio $\rho = \tau_u/\sigma_{mu} = \pi_2^{-1}\pi_6^{-1}\pi_8$:

$$\ell_a=\max\left(\frac{\sigma_{fu}r_f}{\tau_u};\frac{\sigma_{fu}r_f}{\sigma_{mu}}\right) \tag{28}$$

It is obvious that if the bond-strength τ_u is different from the matrix tensile strength σ_{mu}, it will be the lower strength which will determine the minimum required anchorage length ℓ_a. For $\rho=\tau_u/\sigma_{mu}<1$, ℓ_a reflects the critical anchorage length required for a simultaneous fiber yielding and plastic interface sliding, while for $\rho>1$, the interface will behave elastically, as the frictional mechanism will occur in the matrix in a zone close to the interface.

Furthermore, it is instructive to inspect Equations (1) and (2) at the length scale of ℓ_a, by considering the dimensional transform $2z = \ell_a \bar{z}$. For $\rho > 1$, considered in conjunction with Equation (25), the following dimensionless forms of (1) and (2) are obtained:

$$\frac{d\bar{\sigma}_f}{d\bar{z}}=-\bar{\tau}_m(r_f);\quad \bar{\tau}_m=\frac{\tau_m}{\sigma_{mu}} \tag{29}$$

$$\frac{\partial\bar{\sigma}_m}{\partial\bar{z}}=-\frac{1}{2}\frac{\sigma_{fu}}{\sigma_{mu}}\left(\frac{\partial\bar{\tau}_m}{\partial\bar{r}}+\frac{\bar{\tau}_m}{\bar{r}}\right);\quad \bar{\sigma}_m=\frac{\sigma_m}{\sigma_{mu}};\quad \bar{r}=\frac{r}{r_f} \tag{30}$$

We note for large values of σ_{fu}/σ_{mu}, that $\bar{\tau}_m$ still decreases with $1/\bar{r}$, from a maximum value at the fiber-matrix interface, irrespective of the longitudinal stress distribution in the matrix. This stress distribution will only be affected by the radial shear stress distribution when inspecting the matrix behavior on a radial length scale on the order of $r^* = r_f\sigma_{fu}/2\sigma_{mu}$, for which Equation (30) reads:

$$\frac{\partial\bar{\sigma}_m}{\partial\bar{z}}=-\left(\frac{\partial\bar{\tau}_m}{\partial\bar{r}^*}+\frac{\bar{\tau}_m}{\bar{r}^*}\right);\quad \bar{r}^*=\frac{r}{r^*}=\frac{2r\sigma_{mu}}{r_f\sigma_{fu}} \tag{31}$$

For typical values of FRCC and HP2C (Table 1), $\rho \sim 1$, the radial length scale is on the same order of the half the plastic anchorage length, i.e. $r^* \approx \ell_a/2$, thus:

$$\text{FRCC}: r^* = 25-75\text{mm};\ \text{HP2C}: r^* = 5-15\text{mm} \tag{32}$$

Whether or not this length scale affects the mechanical performance of the composite material depends on the average spacing of fibers in the composite, which can be estimated using a representative composite cylinder such as the one shown in Figure 4. The cylinder of the matrix-fiber composite has a radius C and a length (L_f + 2C) which encapsulates a fiber of radius r_f and length L_f. To achieve fiber volume fractions between 1 - 5% requires a composite cylinder radius between 2 – 5 mm (using typical fiber dimensions). The distance between neighboring fibers typically ranges between 2C = 5 – 10 mm. Hence, for FRCC, for which $C \ll r^*$, the stresses in the characteristic cylinder are comprised mostly of shear stresses. Accordingly, failure is confined to the interface region (close to the fiber) in the form of interface failure/fiber slippage. By comparison, in HP2C, C and r* are on the same order of magnitude. This suggests that there is a buildup of normal stresses in the HP2C matrix, which can induce multiple cracking in the matrix. It can also be suggested that this effect partially accounts for the substantial ductility gain of HP2C - in contrast to FRCC - after cracking.

2.4 *Optimal Fiber Radius*

When transverse cracks begin to form in the matrix, the fibers bridge these cracks. If the matrix and reinforcing fibers have not failed, an interfacial crack may form between the fiber and the matrix, which can lead to debonding and pullout of the fiber, and ultimately to the failure of the composite. This proc-

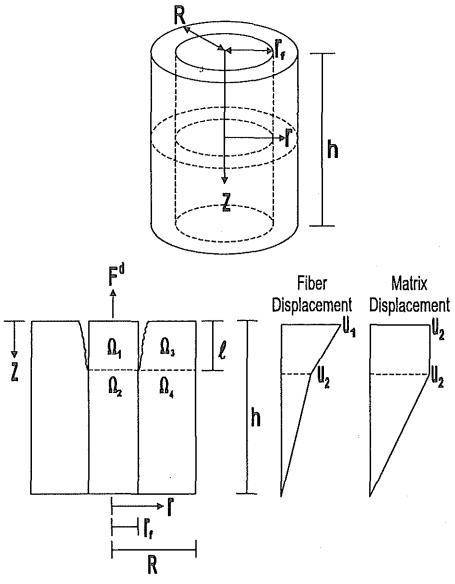

Figure 5. Debonding of Fiber from Matrix

ess can be represented by the interfacial debonding model shown in Figure 5.

In this model, a fiber is pulled out under a longitudinal force of F^d from a representative matrix cylinder of height h and radius R. At the pulled end of the fiber, a debonding zone of length ℓ has formed. In the bonded regime of the fiber, $z > \ell$, the fiber and matrix share the same displacement field, which is approximated to develop linearly from 0 to u_2. In the debonding zone, $z < \ell$, no stresses are transferred from the fiber to the matrix. In this way, the fiber displacement evolves under the load from u_2 to u_1 while the matrix displacement is constant at u_2. That is, frictional stress transfer is ignored. The chosen displacement field is kinematically admissible (satisfies the displacement boundary conditions), which allows us to solve for an upper bound value for the pullout stress in the fiber, p, at unstable debonding. The potential energy, $E_{pot}(\xi')$ of the system is as follows:

$$E_{pot}(\xi') = \frac{\pi(R^2 - r_f^2)}{2(h-\ell)}(\lambda_m + 2\mu_m)u_2^2 + \frac{\pi r_f^2}{2\ell}(\lambda_f + 2\mu_f)(u_1 - u_2)^2 + \frac{\pi r_f^2}{2(h-\ell)}(\lambda_f + 2\mu_f)u_2^2 - F^d u_1 \quad (33)$$

where λ and μ are Lame's material constants and $k' = (\lambda_m + 2\mu_m)/(\lambda_f + 2\mu_f)$. Also note:

$$\lambda_m + 2\mu_m = \frac{E_m(1-\nu_m)}{(1-2\nu_m)(1+\nu_m)} \quad (34)$$

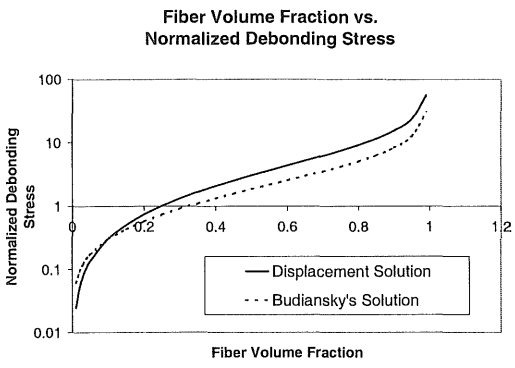

Figure 6. Comparison of Simplified 2-Body Displacement Solution with Budiansky's 3-Body Solution

Minimizing the potential energy with respect to u_1 and u_2 provides a solution for an upper bound estimate of the minimum potential energy, and ultimately to the energy release rate, G, which upon fracture propagation is equal to the fracture energy of the interface, G_f:

$$G = -\frac{\partial E_{pot}}{\partial(2\pi r_f \ell)} = G_f \quad (35)$$

One can then solve the macroscopic stress at fiber pullout $\Sigma = p/V_f$ (with p the fiber pullout stress):

$$\Sigma = 2V_f\sqrt{\frac{G_f(\lambda_f + 2\mu_f)[(1-V_f)k' + V_f]}{r_f k'(1-V_f)}} \quad (36)$$

This solution, based on a simplified kinematically admissible displacement field, is similar to the debonding stress solved by Aveston and Kelly (1973) and later by Budiansky et al. (1985). However, Budiansky used a three-body system taking into account the shear stresses in the interface zone.

Figure 6 compares the derived solution (36) to Budiansky's solution plotting the normalized macroscopic stress, $\bar{\Sigma} = \Sigma(r_f / E_f G_f)^{1/2}$, versus fiber volume ratio, V_f. Comparing the solution given by Budiansky and the solution shown in this section shows that the three-body system exhibits similar behavior as the two-body system, particularly at typical fiber volume ratios of fiber reinforced cementitious composites. This confirms the relevance of the two-body system. Finally, solution (36) is also

Table 2. Typical Values of Length Scales

Length Scale	FRCC Typical Length	HP2C Typical Length
	mm	mm
Elastic Embedment	.5-1	.5-1
Anchorage Strength	50-150	10-40
Radial Influence Zone	25-75	5-15
Optimal Fiber Radius	.005-.2	.01-.5

similar to the one derived by Stang and Shah (1986), based on the compliance method, and on uniaxial matrix and fiber behavior which neglects Poisson effects in the elastic response of matrix and fiber.

Last, an obvious use of the size dependency of the fracture solution (36) is to derive a limiting radius for the fibers (see e.g. Aveston et al., 1971), which ensures an ideal failure of the composite; that is a simultaneous failure of the fiber in yielding and failure of the interface though debonding. Substituting the yield strength of the fiber σ_{fu} into the fiber pullout stress $p = \Sigma V_f$ reveals an optimal fiber radius:

$$r_{fo} = \frac{4V_f^2 G_f (\lambda_f + 2\mu_f)[(1-V_f)k' + V_f]}{\sigma_{fu}^2 k'(1-V_f)} \quad (37)$$

At this optimal fiber radius, simultaneous interface debonding and fiber yielding will occur. For typical material values,

$$\text{FRCC}: r_{fo} = .005 - .2\,\text{mm}; \qquad \text{HP2C}: r_{fo} = .01 - .5\text{mm} \quad (38)$$

In most cases, $r_f >> r_{fo}$ for FRCC implying fiber debonding will occur well before fiber yielding occurs. Therefore FRCC materials are not designed efficiently to dissipate energy through simultaneous fiber yielding and interface debonding. By contrast, HP2C materials have fiber radii of the same magnitude as the optimal fiber radius, $r_f \sim r_{fo}$. Therefore, HP2C materials are better designed to dissipate energy through interface debonding and fiber yielding, which can account for the improved ductility properties of HP2C.

Also note that the interface debonding capacity of the fiber pullout is independent of the length of the fiber. Therefore, it seems unlikely that the interface debonding resistance of the system can be improved with longer fibers.

3 CONCLUSION

The four length scales which are likely to affect the mechanical performance of fiber reinforced cementitious composites are summarized in Table 2. These length scales are related to the transfer of elastic stresses, the anchorage of fibers, the radial influence zone, and the optimal fiber radius, and may serve as guidelines for the optimal design of FRCC and HP2C materials:

- The fiber lengths in FRCC are often insufficient to satisfactorily prevent interface failure and fiber pullout before the maximum capacity of the fibers are achieved. Therefore the fibers in these materials are over-designed. The use of hooked fibers or lower strength fibers could improve this problem. In contrast, HP2C materials can often achieve simultaneous interface failure/fiber yielding (without the use of hooked fibers)– a more efficient use of materials.
- The radial influence zones of fiber pullout in FRCC are much larger than the average distance between fibers. Therefore, only small normal stresses can develop in the matrix while shear stresses at the interface lead to composite failure. This represents an underutilization of matrix strength. By comparison, the loading of fibers in HP2C can often cause tensile stresses in the matrix, which can lead to multiple cracking. This may partially account for the improved ductility behavior of HP2C.
- The radii of fibers in FRCC are often too large to achieve simultaneous debonding/yielding of fibers. Therefore, fibers debond and are pulled out of the matrix well before the strength capacities of the fibers are utilized. This is not the case in HP2C which has fiber radii of the same magnitude of the optimal fiber radius. This induces simultaneous fiber yielding/debonding in HP2C.

In summary, HP2C seems a better suited match of two materials and their interaction. Due to the compatibility of materials in HP2C, failure can occur under multiple modes simultaneously. This allows a higher dissipation of energy and, in turn, a more ductile material behavior.

It should be noted that the considered length scales affect the mechanical behavior only, and do not take into account other aspects of concrete design such as cost and workability.

ACKNOWLEDGEMENTS

The authors would like to thank MIT's Undergraduate Research Opportunity Program (UROP) for their support of this work.

REFERENCES

Aveston, J., Cooper, G., Kelly, A. 1971. The Properties of Fibre Composites. *Conference Proceedings*: 15-24. National Physical Laboratory/IPC Scientific and Technical Press, Teddington.

Aveston, J. & Kelly, A. 1973. Theory of multiple fracture of fibrous composites. *Journal of Materials Science* 8: 352-362.

Barenblatt, G. 1996. *Scaling, self-similarity, and intermediate asymptotics*, Cambridge University Press, NY, USA.

Budiansky, B., Hutchinson, J., Evans, A. 1985. Matrix Fracture in Fiber-Reinforced Ceramics. *Journal of the Mechanics of Physical Solids*, 34(2): 167-189.

Gopalaratnam, V. & Shah, S. 1987. Failure Mechanisms and Fracture of Fiber Reinforced Concrete. Shah and Batson, (eds), *Fiber Reinforced Concrete Properties and Applications*: 1-25. ACI, Detroit, pp.1-25.

Kelly, A. 1964. The strengthening of metals by dispersed particles. *Proceedings of the Royal Society of London. Series A:Mathematical and physical sciences*, 282: 63-79. Royal Society, London.

Leung, C. & Li, V. 1991. New Strength-Based Model for the Debonding of Discontinuous Fibers in Elastic Matrix. *Journal of Material Science* 26(11): 5996-6010.

Lim, T., Paramasivam, P., Lee, S. 1987. Analytical Model for Tensile Behavior of Steel-Fiber Concrete. *ACI Materials Journal* 84(4): 286-298.

Rossi, P., Coussy, O., Boulay, C., Acker, P., Malier, Y. 1986. Comparison Between Plain Concrete Toughness and Steel Fiber Reinforced-Concrete Toughness. *Cement and Concrete Research* 16(3): 303-313.

Rossi, P. 1997. High Performance Multimodal Fiber Reinforced Cement Composites (HPMFRCC): The LCPC Experience. *ACI Materials Journal* 94(6): 478-483.

Shao, Y., Ouyang, C., Shah, S. 1998. Interface Behavior in Steel Fiber/Cement Composites under Tension. *Journal of Engineering Mechanics* 24(9): 1037-1044.

Soroushian, P. & Bayasi, Z. 1987. Prediction of the Tensile Strength of Fiber Reinforced Concrete: a Critique of the Composite Material Concept. Shah and Batson (eds), *Fiber Reinforced Concrete Properties and Applications*: 71-84. ACI, Detroit.

Stang, H. & Shah, S. 1986. Failure of fibre-reinforced composites by pull-out fracture. *J. Mater. Sci.* 21(3): 953-957.